Direct Observation of Coulomb Crystals and Liquids in Strongly Coupled rf Dusty Plasmas

J. H. Chu and Lin I

Department of Physics, National Central University, Chungli, Taiwan 32054, Republic of China

(Received 18 January 1994)

The strongly coupled dusty plasmas are formed by suspending negatively charged SiO_2 fine particles with 10 μm diameter in weakly ionized rf Ar discharges. The Coulomb crystals and liquids are directly observed for the first time using an optical microscope. By properly controlling the system parameters, hexagonal, fcc, and bcc crystal structures and solids with coexisting different crystal structures can be formed. Increasing the rf power causes the transition to the more disordered liquid state.

PACS numbers: 64.70.Dv, 52.55.Mg, 52.90.+z, 82.70.Dd

A plasma is a statistical system of mobile charged particles interacting with each other through electromagnetic forces. A plasma with coupling constant Γ, defined as the ratio of the average Coulomb energy to the average thermal energy, greater than unity may be called strongly coupled plasma [1]. The strongly coupled plasma exhibits interesting phenomena such as the formation of the liquid and solid structures [1]. However, most of the classical laboratory plasmas are weakly coupled. For example, $\Gamma \sim 10^{-3}$ and 10^{-5} for typical glow discharges and thermonuclear fusion plasmas, respectively. The requirements of very high density and low temperature make it difficult for the formation of the liquid and solid structures in laboratory plasmas.

If fine particles are introduced into the plasma, a dusty plasma system can be formed. The particles can be negatively charged due to the higher mobility of electrons than ions in the plasma, and suspended in the plasma which floats positively with respect to the container [2–4]. For example, a micron size particle in a typical glow discharge system can be easily charged to 10^3 electrons. Since Γ is proportional to the square of the charges on the particle, it can be significantly increased to greater than unity. Ikezi and Forouki and Hamaguchi have demonstrated the possibility of forming Coulomb solid in dusty plasma systems through their calculation and computer simulation [4,5]. In this Letter, we report the first direct experimental observation of the Coulomb liquid and crystals with different structures using an optical microimaging system in a strongly coupled dusty plasma system.

Coulomb crystals and liquids have also been observed in other similar strongly coupled Coulomb systems such as charged dust particles in the electrostatic vacuum trap [6], stored laser-cooled Be and Mg ion clusters in the Paul and Penning traps [7], and liquid with charged colloidal suspensions [8–12]. In the liquid system, charged colloids are also coupled through Yukawa type repulsive force. Crystals with different structures are formed in the oppositely charged liquid background. In the dusty plasma system, although the screened Coulomb interaction is similar, the gaseous background is much less viscous and dissipative than the dense liquid which usually overdamps the particle motion. The plasma also supports self-excited electric field fluctuations which in turn affects the particle motion [13,14]. Unlike the complicated processes of changing the densities of particles and electrolyte or introducing shear force for liquid colloidal systems [9–12], the crystal in the dusty plasma can be melted by directly varying the control parameter which decreases the relative strength of the Coulomb coupling. Therefore, the dusty plasma provides a new system for the study of crystal dynamics and the melting process. For particle size exceeding 1 μm, the dynamical behaviors can be directly monitored using an optical microscope.

The early research on dusty plasma systems mainly concentrated on the astrophysical plasma systems at low Γ [3]. In the past several years, motivated by the application of fine particles and the contamination control for the microelectronic material processes, the particle formation, transport, trapping, manipulation, and their effects on the discharge properties have been studied in glow discharge dusty plasma systems [15–17]. However, the collective behaviors are less well studied in laboratories.

In our previous works, we have studied and developed the SiO_2 particle fabrication process through homogeneous reactions between silane and oxygen in the rf Ar discharge, and demonstrated the formation of amorphous Coulomb solid with polydispersive particle size distribution and the response of particle motion to electric field fluctuations [13,18]. In this study, an electrostatic trap with better symmetry is designed to confine the dusty plasma. We are able to form and observe colloidal liquids and crystals in the trap by precisely controlling the rf power.

The experiment was conducted in a cylindrical symmetric rf plasma system as described in our preliminary report [19]. Figure 1 shows the side view of the system. It consists of a hollow outer electrode capacitively coupled to a 14 MHz rf power amplifier, a grounded center electrode with a ring-shape groove on the top for particle trapping, and a top glass window for observation. The system is pumped by a diffusion pump. O_2 and SiH_4 are introduced into the chamber with 10 mTorr background argon gas. The reactive gas flow rate to the partial pressure ratio is 0.2 sccm/mTorr (sccm stands for cubic cen-

0031-9007/94/72(25)/4009(4)$06.00

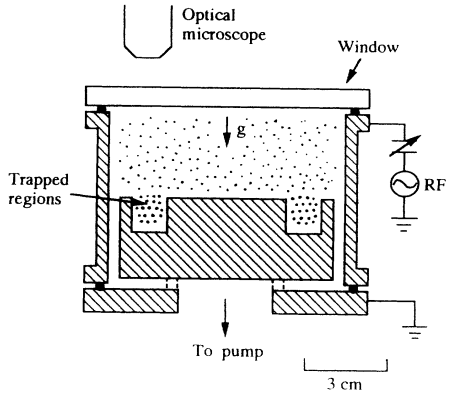

FIG. 1. Sketch of the side view of the cylindrical discharge system.

timeter per minute at standard temperature and pressure). The O_2 to SiH_4 partial pressure ratio and rf power are kept at 1 and 30 W, respectively, and the system total pressure is below 10 mTorr for particle generation. An axial magnetic field (50 to 100 G) is also introduced to increase the generation efficiency. The particle size and number density increase with the reactive gas flow on-time and pressure. After the formation of micron size particles, the reactive gas flows and the magnetic field are turned off. Particles can be very well trapped in the toroidal groove. Under the gravitational force, the particle diameter slowly increases with the decreasing height. Particle size is almost monodispersive within 3 mm along the vertical direction. The rf power precisely controlled by a programmable function generator is the main control parameter. A digital video recording system is used to monitor the image of the particles illuminated by a He-Ne laser through an optical microscope mounted on the top of the chamber. The optical axis is parallel to the symmetry axis of the system.

As we decrease the rf power to about 1 W at 200 mTorr argon pressure, the formation of different colloidal crystals is observed in the groove region. For example, Fig. 2(a) shows the hexagonal crystal structure. The laser light is shining downward from the right to the left with 45° incident angle and with a Gaussian type intensity distribution. Therefore, the particle images are brighter and seem to be larger at the center part of the picture due to the stronger scattered light. The two pictures in Fig. 2(a) are taken at 1 sec intervals. The structure is stationary except the small fluctuations around the equilibrium positions. Figure 3(a) shows the magnified version of the hexagonal structure. The optical axis is normal to the graded plane in the sketch. The optical depth of our microscope is slightly longer than the distance between the two adjacent lattice planes. The slight fluctuations of particle positions from the vertical crystal axis for the particles in the adjacent lattice plane causes the appearance of pairs of particles with small separations. The blurred images are from the particles in the

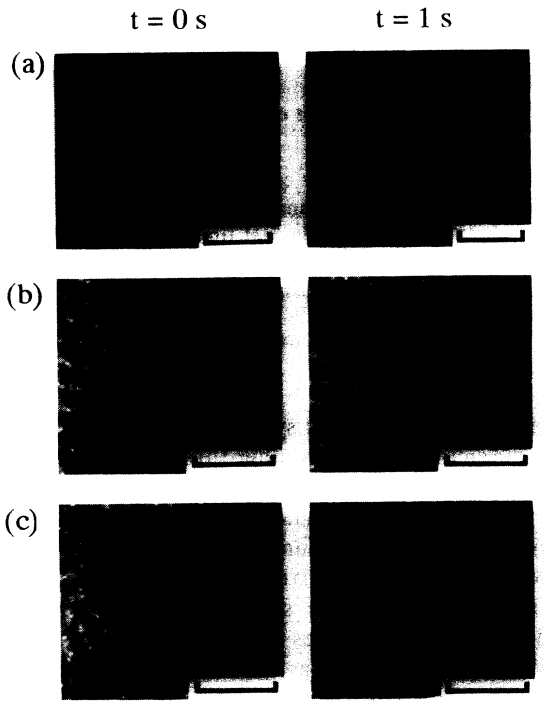

FIG. 2. Micrographs of the hexagonal structure and the more disordered structures at different rf power. (a) 1 W. (b) 2 W. (c) 3 W. The pictures in the right column are taken 1 sec after those in the left column, respectively. The bars correspond to 500 μm.

third plane. Curve a in Fig. 4 shows the 2d pair distribution function $g(r)$ in the horizontal plane of the hexagonal structure, which is obtained by directly measuring the distance between particles. Fifty picture frames are used for averaging. The sharp first peak and the following peaks with slowly descending heights located at $\sqrt{3}$, 2, $\sqrt{7}$, ... times the location of the first peak, as indicated by the arrows, manifest the hexagonal structure.

Increasing rf power increases the amplitude of fluctuations. It also causes the presence of pairs of the neighboring particles from the two adjacent planes with larger separations. Figure 2(b) shows the more disordered structure at 1 sec intervals and 2 W rf power. The short range order still exists. Figure 2(c) shows the liquid structure at 1 sec intervals and 3 W rf power. Curves b and c in Fig. 4 are the $g(r)$ of the states in Figs. 2(b) and 2(c), respectively. The peaks are shorter and broader as the state becomes more disordered. The short range order of the liquid structure is evidenced by the first broad peak and the fast descending following peaks.

In the solid phase, bcc and fcc structures can also be prepared at low rf power. Figure 3(b) shows the bcc structure. The structure can be identified by carefully comparing the slight difference of the images of the particles located in different lattice planes while slowly varying the height of the microscope. For a rectangle formed by nine near neighbor particles in the picture, the four

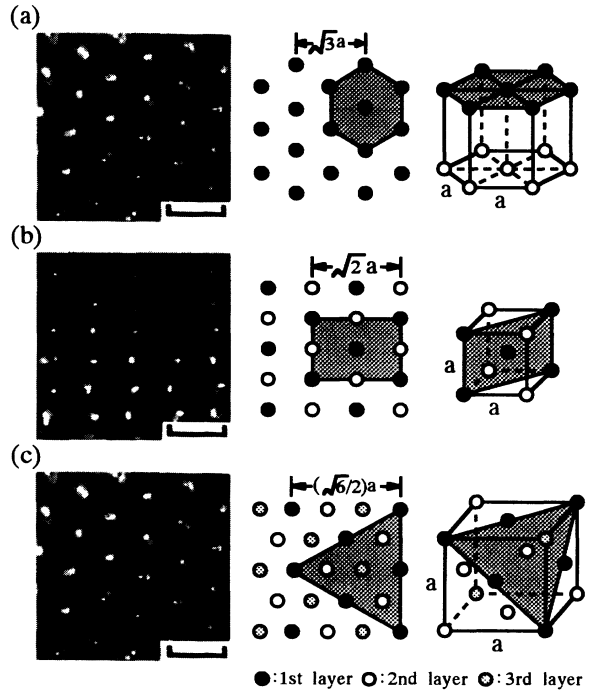

FIG. 3. Micrographs and sketches of the different crystal structures. (a) Hexagonal; (b) bcc; (c) fcc. The center column corresponds to the structures in the micrographs. The graded areas in the sketches are normal to the optical axis. The bars correspond to 200 μm.

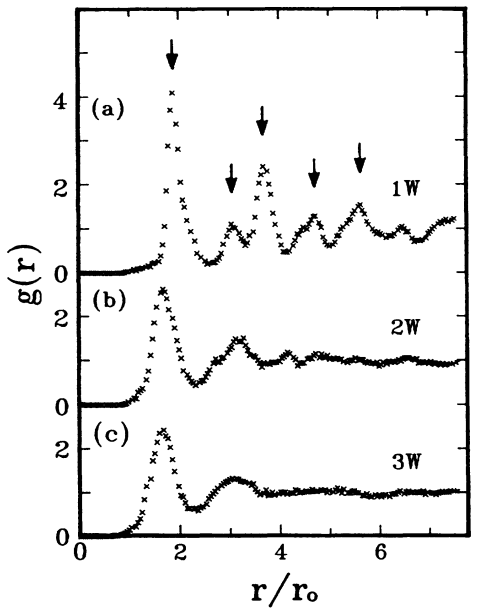

FIG. 4. The 2d radial pair distribution functions of the structures at different rf power, where r_0 is the Wigner-Seitz radius [1]. The arrows from left indicate the positions of the successive nearest neighbors for a hexagonal lattice. The curves *a*, *b*, and *c* correspond to the states in Figs. 2(a), 2(b), and 2(c), respectively.

corner particles and the one located at the center are in the same lattice plane. The remaining four particles at the centers of the four sides are located in the next plane. The aspect ratio of the rectangle is very close to $\sqrt{2}$. This structure periodically repeats as the height of the microscope is varied, and it corresponds to the bcc structure with the (110) direction along the optical axis. The lattice constant a is about 200 μm which is also about $\sqrt{2}$ times the distance between the two horizontal planes. Figure 3(c) shows the fcc structure with the (111) direction pointing along the optical axis. The blurred images are from the particles in the third plane. With a similar method, the fcc structure can be easily identified. By properly adjusting the plasma parameters, hcp (hexagonal closed-packed) structure could also be obtained (not shown) [19].

In the solid phase, we have also observed different defects and the coexisting domains with different crystal structures. For example, Fig. 5(a) shows that the bcc structure coexists with the fcc structure at the lower left corner. Figures 5(b), 5(c), and 5(d) are sequentially taken at 1, 3, and 5 sec later, respectively. The domain boundary moves with a nonconstant speed.

In our trap, the particle diameter, particle density, ion density, electron temperature, and ion temperature are about 10 μm, 2×10^5 cm^{-3}, 10^9 cm^{-3}, 2 eV, and 0.03 eV, respectively from our microimage and Langmuir probe measurements. According to Ikezi [4], it falls in the right regime in which the Coulomb solid ($\Gamma \geq 170$) can be formed. The Γ of our solid is about a few hundred according to our rough estimate. Unlike the cubic lattice from the computer simulation by Farouke and Hamaguchi [5], the formation of the bcc, fcc, and hcp structures and the phase with coexisting different structures in our system are very similar to those observed in other liquid systems with colloidal suspensions [8,10–12]. The obser-

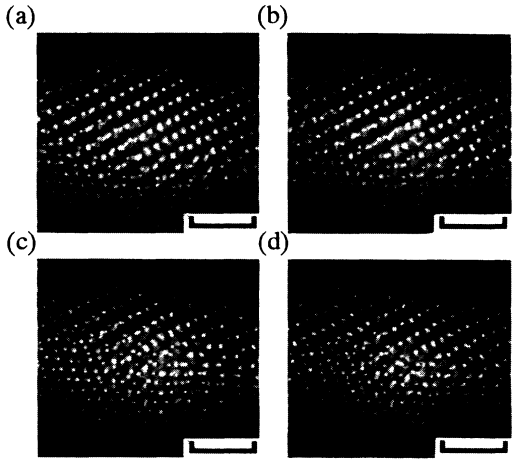

FIG. 5. The states with coexisting bcc (upper right) and fcc (lower left) structures sequentially taken at 0, 1, 3, and 5 sec, respectively. The bars correspond to 500 μm.

vation of the hexagonal structure which is supposed to be unstable for a large N system with repulsive interaction is interesting. The roles played by the confinement of the trap (the groove width is about 50 times the lattice constant, and the particles are pushing inward by the electric field in the sheath) and the vertical gravitational force need to be further investigated. Increasing rf power increases ion density which weakens the Coulomb coupling through the increasing Debye screening, and causes the melting of the solid [4]. The $g(r)$ of our liquid phase is similar to that with Γ about one hundred in the simulation [1]. It is interesting to note that our system has a much faster response (less than 1 sec) to the change of the control parameter than the liquid colloidal system. Interesting dynamical phenomena in the melting and solidification processes such as the formation of small crystal domains surrounded by disorder structures and the exchange of the positions of neighboring particles have also been observed in our system. The details are under intensive investigation and will be reported shortly.

In conclusion, we have demonstrated the formation of the Coulomb crystals and liquids in a strongly coupled dusty plasma system using the direct optical microimaging system. SiO_2 particles with 10 μm diameters are generated chemically and suspended in our toroidal trap. At low rf power, hexagonal, fcc, and bcc structures, coexisting domains with different crystal structures and propagating domain boundary, and other rich phenomena are observed. Increasing the rf power causes the melting of the crystal. The convenient control of the system parameter, the less viscous motion of particles in the gaseous background, and the right particle size for direct optical imaging open a new environment for the study of the strongly coupled plasma system.

The authors would like to thank Dr. M. O. Robbins and Dr. S. K. Lai for discussions. This work is supported by the Department of Physics, National Central University and the National Science Council of the Republic of China under Contract No. NSC82-0201-M008-118.

[1] S. Ichimaru, Rev. Mod. Phys. **54**, 1017 (1982).
[2] M. S. Barnes, J. H. Keller, J. C. Forster, J. A. O'Neil, and D. K. Couttas, Phys. Rev. Lett. **68**, 313 (1992).
[3] C. K. Goertz, Rev. Geo. Phys. **27**, 271 (1989).
[4] H. Ikezi, Phys. Fluids **29**, 1764 (1986).
[5] R. T. Farouki and S. Hamaguchi, Appl. Phys. Lett. **61**, 1973 (1992).
[6] R. F. Wuerker, H. Shelton, and R. V. Langmuir, J. Appl. Phys. **30**, 342 (1959).
[7] F. Diedrich, E. Peik, J. M. Chen, W. Quint, and W. Walter, Phys. Rev. Lett. **59**, 2731 (1987); I. Waki, S. Kassner, G. Birkl, and H. Walther, Phys. Rev. Lett. **68**, 2007 (1992).
[8] N. A. Clark, A. J. Hurd, and B. J. Ackerson, Nature (London) **281**, 57 (1979).
[9] D. H. Van Winkle and C. A. Murry, Phys. Rev. A **34**, 362 (1986).
[10] K. Ito, H. Nakamura, and N. Ise, J. Chem. Phys. **85**, 6136 (1986).
[11] K. Kremer, M. O. Robbins, and G. S. Grest, Phys. Rev. Lett. **57**, 2694 (1986).
[12] E. B. Sirota, H. D. Ou-Yang, S. K. Sinka, and P. M. Chaikin, Phys. Rev. Lett. **62**, 1524 (1989).
[13] J. H. Chu, J. B. Du, and Lin I, J. Phys. D **27**, 296 (1994).
[14] J. H. Chu and Lin I, Phys. Rev. A **39**, 233 (1989).
[15] G. S. Selwyn, J. Singh, and R. S. Bennett, J. Vac. Sci. Technol. A **7**, 2758 (1989).
[16] J. E. Daugherty, R. K. Porteous, M. D. Kilogre, and D. B. Graves, J. Appl. Phys. **72**, 3934 (1992).
[17] M. J. McCaughey and M. J. Kushner, J. Appl. Phys. **69**, 6952 (1991).
[18] J. H. Chu and Lin I, J. Appl. Phys. **74**, 4741 (1993).
[19] J. H. Chu and Lin I, in Proceedings of the Taipei International Conference on Statistical Physics (to be published).

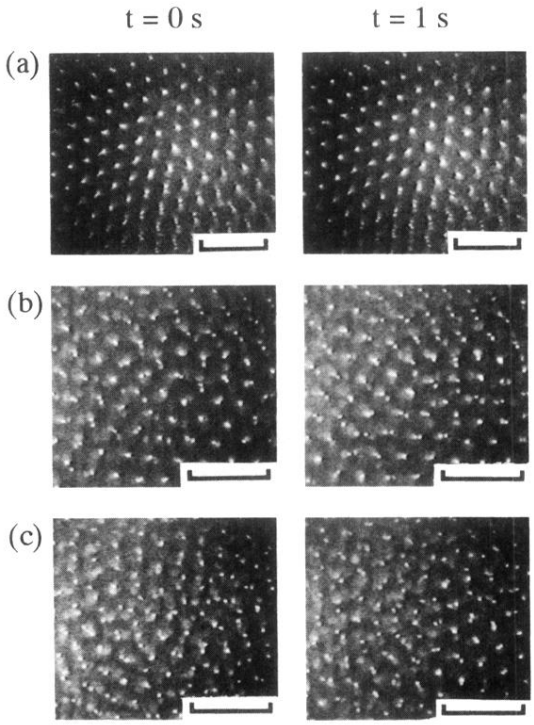

FIG. 2. Micrographs of the hexagonal structure and the more disordered structures at different rf power. (a) 1 W. (b) 2 W. (c) 3 W. The pictures in the right column are taken 1 sec after those in the left column, respectively. The bars correspond to 500 μm.

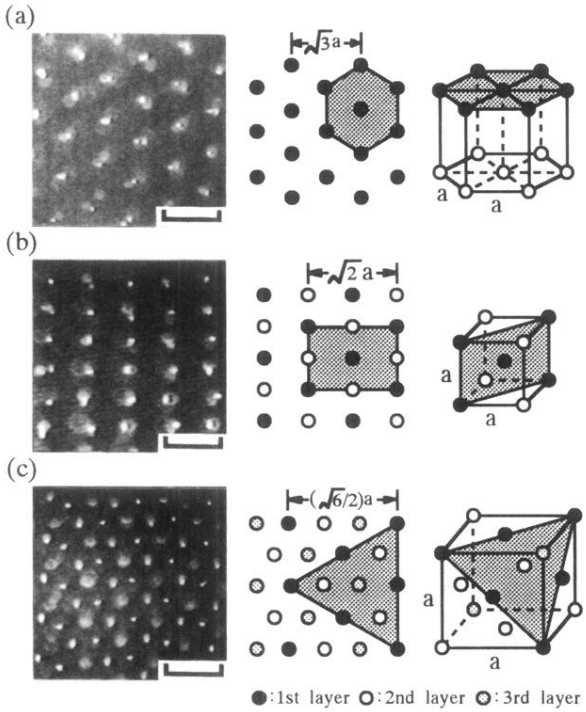

FIG. 3. Micrographs and sketches of the different crystal structures. (a) Hexagonal; (b) bcc; (c) fcc. The center column corresponds to the structures in the micrographs. The graded areas in the sketches are normal to the optical axis. The bars correspond to 200 μm.

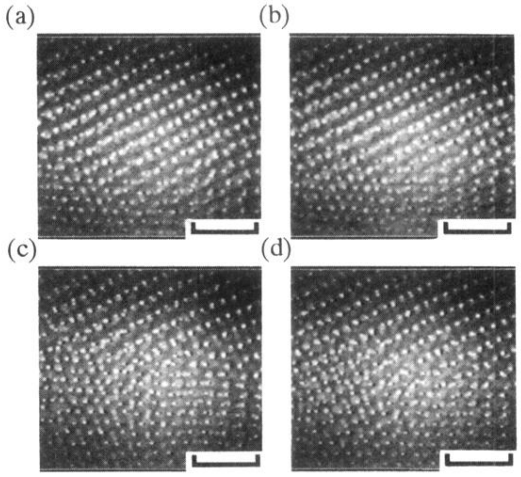

FIG. 5. The states with coexisting bcc (upper right) and fcc (lower left) structures sequentially taken at 0, 1, 3, and 5 sec, respectively. The bars correspond to 500 μm.